

Mitral Valve Patient-Specific Finite Element Modeling from Cardiac MRI: Application to an Annuloplasty Procedure

MARCO STEVANELLA,¹ FRANCESCO MAFFESSANTI,¹ CARLO A. CONTI,¹ EMILIANO VOTTA,¹ ALICE ARNOLDI,² MASSIMO LOMBARDI,³ OBERDAN PARODI,^{4,5} ENRICO G. CAIANI,¹ and ALBERTO REDAELLI¹

¹Bioengineering Department, Politecnico di Milano, Via Golgi 39, 20133 Milan, Italy; ²CILEA, Segrate, MI, Italy; ³Fondazione “G. Monasterio” CNR-Regione Toscana, Pisa, Italy; ⁴CNR Institute of Clinical Physiology, Pisa, Italy; and ⁵CNR Institute of Clinical Physiology, Milan, Italy

(Received 7 September 2010; accepted 15 December 2010; published online 4 January 2011)

Associate Editor Bruce H. KenKnight oversaw the review of this article.

Abstract—We aim at testing the possibility to build patient-specific structural finite element models (FEMs) of the mitral valve (MV) from cardiac magnetic resonance (CMR) imaging and to use them to predict the outcome of mitral annuloplasty procedures. MV FEMs were built for one healthy subject and for one patient with ischemic mitral regurgitation. On both subjects, CMR imaging of 18 long-axis planes was performed with a temporal resolution of 55 time-frames per cardiac cycle. Three-dimensional MV annulus geometry, leaflets surface and PM position were manually obtained using custom software. Hyperelastic anisotropic mechanical properties were assigned to MV tissues. A physiological pressure load was applied to the leaflets to simulate valve closure until peak systole. For the pathological model only, a further simulation was run, simulating undersized rigid annuloplasty before valve closure. Closure dynamics, leaflets stresses and tensions in the subvalvular apparatus in the healthy MV were consistent with previous computational and experimental data. The regurgitant valve model captured with good approximation the real size and position of regurgitant areas at peak systole, and highlighted abnormal tensions in the annular region and sub-valvular apparatus. The simulation of undersized rigid annuloplasty showed the restoration of MV continence and normal tensions in the subvalvular apparatus and at the annulus. Our method seems suitable for implementing detailed patient-specific MV FEMs to simulate different scenarios of clinical interest. Further work is mandatory to test the method more deeply, to reduce its computational time and to expand the range of modeled surgical procedures.

Keywords—Mitral valve, Annuloplasty, Surgical planning, Finite element modelling, Cardiac magnetic resonance.

INTRODUCTION

The mitral valve (MV) is a complex apparatus composed of four principal substructures: mitral annulus (MA), leaflets, chordae tendineae and papillary muscles (PMs). Their synergic action regulates the normal valvular function, thus preventing the backflow of blood from the left ventricle to the left atrium. During systole, when the left ventricular pressure raises, the annulus shrinks and PMs contract, tightening the chordae tendineae and driving correct leaflets coaptation and complete closure of the orifice.

Several mechanisms can alter the proper mitral function and lead to mitral regurgitation (MR). Primary (or organic) disease is intrinsic to the valvular tissue, and includes myxomatous degeneration, rheumatic disease, endocarditis, and fibro-elastic degeneration. Secondary (or functional) MR is the result of the alteration of a normal mitral apparatus because of an altered ventricular geometry, due to ischemia or dilated cardiomyopathy.

In particular, in the present study we analyzed a pathological MV affected by ischemic MR. Ischemic MR occurs in approximately 20–25% of patients after myocardial infarction and in 50% of those with post-infarct congestive heart failure.⁴ The main alterations include post-ischemic LV remodelling with PMs displacement and leaflet tethering, PMs dysfunction and dyssynchrony, and annular enlargement.

Mitral valve repair is now the most common surgical procedure for MV disease, and involves several techniques that modify MV sub-structures. Restrictive annuloplasty, consisting in the reduction of native MV orifice by insertion of a prosthetic ring of undersized dimensions on the MA, has become the surgical

Address correspondence to Marco Stevanella, Bioengineering Department, Politecnico di Milano, Via Golgi 39, 20133 Milan, Italy. Electronic mail: marco.stevanella@mail.polimi.it

technique of choice for the treatment of ischemic MR.⁵ This trend has encouraged the design of newer and more sophisticated techniques and implantable devices. However, different studies reported a high rate of persistent and recurrent ischemic MR after restrictive annuloplasty. In the early postoperative phase, 15–30% of patients experienced return of MR¹⁸; in addition, even mild residual MR contributes to further LV negative remodelling and increased tethering.⁶

Accordingly, the optimization of these devices and techniques would benefit from quantitative decision support tools allowing cardiac surgeons to test *ex ante* the effects of a given surgical procedure on MV biomechanics.

From this standpoint, MV finite element models (FEMs) could be a valuable tool, since they allow the virtual simulation of a hypothetical scenario and the assessment of the associated MV biomechanics. FEMs have already proven useful in analysing MV biomechanics in physiological and pathological conditions,^{13,15,19,24} in inferring about the relation between tissue microstructure and valve function,^{10,21} and in identifying a rationale in surgical repair procedures.^{2,14,23} Still, the mentioned studies used simplified MV geometrical models representing the average case for a given scenario. Moreover, their implementation required the expertise of scientists with a solid background in continuum mechanics. Thus, none of the referred models fulfilled two mandatory conditions in order to be compatible with the use by clinicians in their current practice: being patient-specific, and being readily set and usable in a semi-automated, fast and user friendly fashion.

To overcome these limitations, our group proposed to build patient-specific MV FEMs from transthoracic real-time three-dimensional echocardiographic (TT-RT3DE) data, thus obtaining several details on the MV end-diastolic real geometry, as well as on the annular dynamics due to the contraction of the surrounding myocardium.²⁴ These details were combined with the description of non-linear and anisotropic tissue response to obtain a realistic MV FEM.

Moreover, a graphical user interface was built to allow users with no engineering background to semi-automatically implement the MV FEM and to run simulations on remote high performance hardware, drastically reducing computation times.¹

In this manuscript we propose the evolution of that work, introducing two main innovations. First, we used cardiac magnetic resonance (CMR) instead of TT-RT3DE as source of data, thus obtaining images with higher time resolution and better blood-to-tissue contrast.^{8,25} This feature allowed us to capture the

complete end-diastolic profile of the MV leaflets, and the time-dependent position of PM tips throughout the cardiac cycle, otherwise unavailable using TT-RT3DE. Second, after testing our procedure on a single healthy MV, we applied it to the prediction of the effects of undersized annuloplasty on a regurgitant MV, in order to test its potential as a predictive tool in this simple but very common MV repair procedure.

MATERIALS AND METHODS

Two models were built using our custom software, respectively for a healthy MV (model-H) and for a patient with ischemic MR associated to ventricular dilation (model-R). With model-H, only one simulation was run (simulation-H), in which valve closure from end diastole (ED) to peak systole (PS) was reproduced. With model-R, two simulations were run, to reproduce valve closure from ED to PS in pre-operative conditions (sim-R_{pre}) and after undersized annuloplasty with a rigid ring (sim-R_{post}). All simulations were performed using the commercial solver ABAQUS/Explicit 6.9-1 (SIMULIA, Dassault Systèmes). The set up of the models and simulations was defined as follows.

Cardiac Magnetic Resonance Acquisition and Processing

On one subject with no valvular defects and on one patient with ischemic MR, CMR imaging of 18 evenly rotated long-axis (one every 10°) planes was performed. Time resolution was equal to 55 frames/cardiac cycle, spatial resolution to 0.78 mm, and slice thickness to 8 mm (Fig. 1a).

For every frame, in each cut-plane the valvular substructures were manually defined (Fig. 1b) using custom software implemented in MATLAB (The MathWorks Inc., Natick, MA, United States): (1) two annular points were identified at the level of leaflet insertions; (2) multiple points defining each leaflet profile were selected and connected through cubic splines; (3) a point was marked for each visible PM tip. The three-dimensional coordinates of the points on each cut-plane were reconstructed from the position of the latter with respect to the rotation axis. The annular profile was then reconstructed by approximating the selected annular points with a 13th order Fourier function; this choice was empirically determined as an adequate trade-off between over-fitting and excessive simplification of MA geometry. Finally, each leaflet surface was obtained via Delaunay tessellation of leaflet profile points (Fig. 1c).

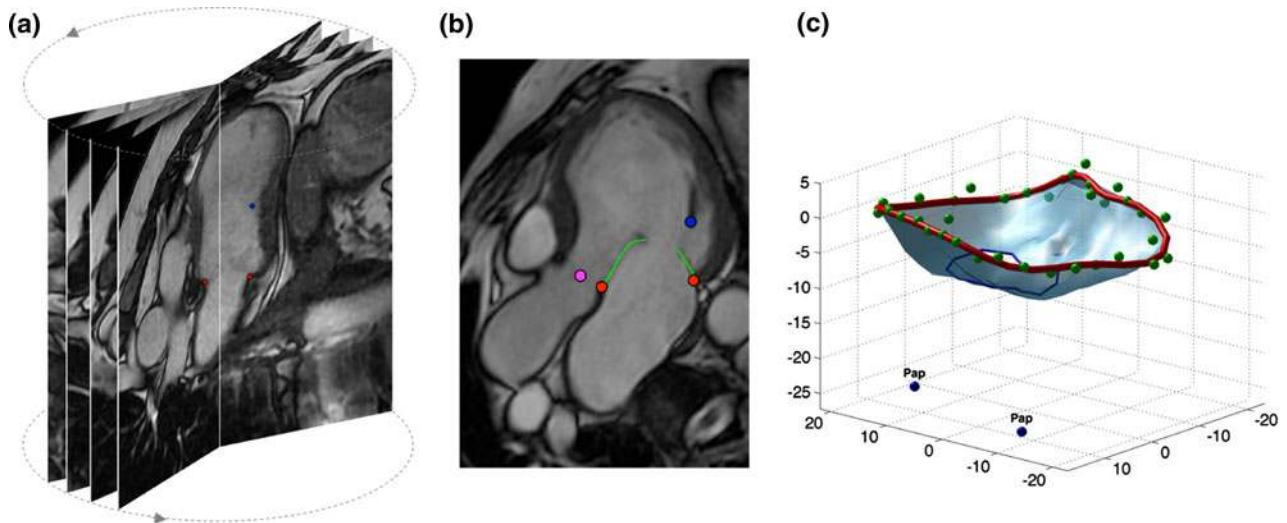


FIGURE 1. (a) acquired long-axis multiple CMR cut-planes; (b) tracing of annulus (red), leaflet (green), papillary muscle tip (blue) and position of the aorta (pink) on a cut-plane; (c) annulus and leaflets profile as reconstructed in 3D through custom software.

MV Geometrical Model

The ED configuration of the MV was assumed as its unloaded one, and the corresponding geometry was reconstructed.

The reconstructed continuous annular profile was sampled in order to define the nodes to be used as seeding for the subsequent discretization of the MV leaflets geometry. Leaflets free margin was defined as a spline function sampled as the annulus; its shape and location were set consistently with CMR data. The leaflets surface limited by the annulus and the free margin was then discretized into a mapped mesh of linear triangular shell elements (ABAQUS S3 shell element type). A regionally varying thickness distribution was assigned to the leaflets, consistently with the one proposed in Kunzelman *et al.*,¹⁵ with a maximum thickness around the fibrous trigones (1.69 mm), an average value of 1.32 mm and 1.26 mm on the anterior and posterior leaflets, respectively.

For each PM, a point cloud was obtained from the selection made on the different cut-planes. In order to define the corresponding geometrical model for PM tips, for each PM a circumference of 3 mm radius was centered in the center of mass of the point cloud and oriented parallel to the valvular plane (i.e. the least square plane approximating the annular profile). Thirteen points were defined on each circumference as the origins of the chordae tendineae, according to a general pattern suggested by expert surgeons, as shown in Fig. 2.

Chordae tendineae of three orders were modeled as truss elements (ABAQUS T3D2 element type); their number, the corresponding branched structure, the origin from PMs and insertion sites on the leaflets were

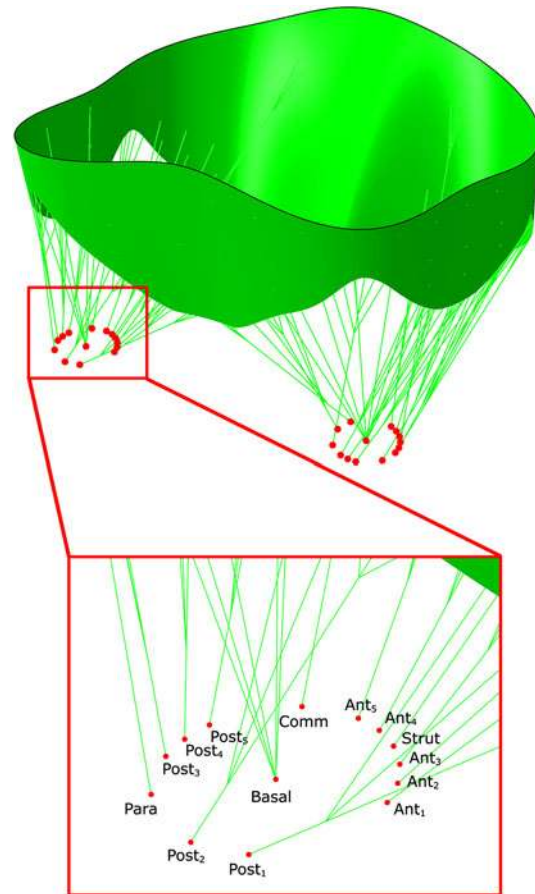


FIGURE 2. (Top) Papillary muscle circumferences with chordal origins. (Bottom) Close-up view of antero-lateral PM chordal origins classified by chordal type: chordae inserting in the anterior leaflet rough zone (Ant), strut chordae (Strut), commissural chordae (Comm), chordae inserting in the posterior leaflet rough zone (Post), paracommissural chordae (Para) and basal chordae (Basal).

defined in accordance to *ex vivo* findings¹⁶ and indications by clinicians. In particular, we included:

- 10 chordae tendineae inserting in the rough zone of the anterior leaflet. These chordae split soon after their origin into three branches: the first branch inserts into the free margin of the leaflet (marginal chorda), while the other two (second-order chordae) insert near the closure line, and between the closure line and the free margin, respectively;
- 2 strut chordae, which are the two thickest chordae inserting in the MV, branching before inserting into the anterior leaflet;
- 2 commissural chordae that branch radially from the main stem with a “fan” shape, and insert into the free margin of the commissural regions;
- 10 chordae tendineae inserting in the rough zone of the posterior leaflet, with the same branching pattern as the anterior ones;
- 2 paracommissural chordae, fan-shaped and inserting into the free margin of the paracommissures separating the three scallops of the posterior leaflet.
- 13 basal chordae, modeled as non-branched chordae, inserting in the basal portion (i.e. near the annular attachment) of the posterior leaflet.

Basal chordae were the only chordal type modeled without strictly mimicking their number and morphology as reported in Lam *et al.*¹⁶; both aspects have considerable inter-subject variability and, thus, could not be reproduced through a paradigm of general validity. Instead, a set of chordae with an equivalent function was defined on the basis of preliminary simulations.

The three-dimensional geometrical models of healthy and regurgitant valve obtained through the described procedure are depicted in Fig. 3.

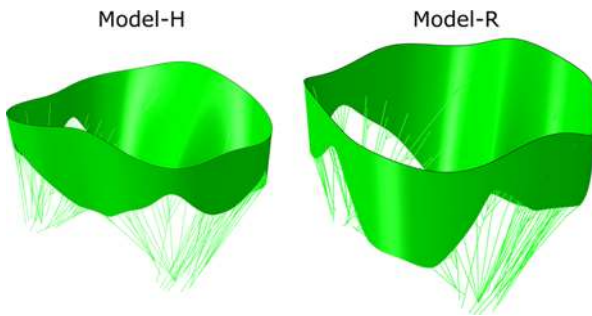


FIGURE 3. Finite element models obtained from the MV reconstruction algorithm for the healthy valve (Model-H) and the regurgitant one (Model-R).

Tissue Mechanical Properties

All tissues were assumed non-linear and elastic. Leaflets behavior was described through the hyperelastic and transversely isotropic constitutive model proposed by May-Newman and Yin,¹⁷ in which the mechanical response in the direction of the collagen fibers (i.e. parallel to the annulus) is much stiffer than the one in transversal direction (i.e. perpendicular to the annulus). This constitutive model is based on a strain energy function ψ that depends on two invariants of strain, I_1 and I_4 :

$$\psi(I_1, I_4) = c_0 \left[e^{c_1(I_1-3)^2 + c_2(\sqrt{I_4}-1)^4} - 1 \right] \quad (1)$$

where $I_1 = \text{tr}(\mathbf{C})$ and $I_4 = \mathbf{a}_0 \cdot \mathbf{C} \cdot \mathbf{a}_0 = \lambda^2$, in which $\mathbf{C} = \mathbf{F} \cdot \mathbf{F}^T$ is the right Cauchy-Green tensor, \mathbf{a}_0 is the unit vector that defines the preferential direction of the fibers in the material in the reference configuration, and λ is the stretch of the fibers in the \mathbf{a}_0 direction. \mathbf{F} is the deformation gradient tensor, defined as $\mathbf{F} = \partial \mathbf{x} / \partial \mathbf{X}$ (i.e. the derivative of the current position as regards to the reference position). In Eq. (1), the term $(I_1 - 3)^2$ is related to the isotropic response of the elastin matrix, while the term $(\sqrt{I_4} - 1)^4$ accounts for the collagen fibers response and it is activated only if $I_4 \geq 1$. The incompressibility condition implies that $J = \det \mathbf{F} = 1$. The constitutive parameters were $c_0 = 0.399$ kPa, $c_1 = 4.325$, $c_2 = 1446.5$ for the anterior leaflet and $c_0 = 0.414$ kPa, $c_1 = 4.848$, $c_2 = 305.4$ for the posterior leaflet,¹⁷ where c_1 and c_2 are dimensionless.

Chordae tendineae response was assumed isotropic and described through hyperelastic models available in ABAQUS/Explicit; for second order chordae, a fifth-order Ogden strain energy function was used, while for all the other chordal types a second order polynomial strain energy function was adopted. For each chordal type, constitutive parameters were defined via interpolation of uniaxial test data obtained from literature.¹² Constant cross-sectional area values of 0.40, 1.15 and 0.79 mm² were assigned to marginal, strut and basal chordae, respectively. The density assumed for all valvular tissues was equal to 10.4 g/cm³, a value ten times higher than the real one, to take into account the inertial effects of the blood moved by MV leaflets during closure.²³

Boundary Conditions

In simulation-H and simulation-R_{pre}, throughout a single step of 1.0 s, the motion of MA and PMs derived from CMR was modeled via kinematic boundary conditions, i.e. imposing time-dependent nodal displacements derived from annular nodes position at each time-frame of the CMR dataset. A physiological

transvalvular pressure drop, up to 120 mmHg, was applied on the ventricular side of the leaflets.

Following a previously adopted rationale,²³ simulation- R_{post} was a two-step simulation. In the first step, no pressure loads were applied and PM translations were constrained. Displacements were imposed to the nodes on the annulus, whose original commissure-commissure diameter was of 45 mm, to adapt its shape to the profile of a 40 mm total rigid ring, representative of the most commonly implanted type of annular prostheses.³ This ring had a D-shaped design, with the straight portion of the D corresponding to the anterior portion of the ring, an approximately 4:3 ratio between commissural and septo-lateral ring diameters, and a slightly non-planar profile. Nodal displacements were set assuming that the change in annular length was uniform in the intertrigonal tract of the annulus and in the posterior one.

In the second step, the obtained annular shape was maintained, PMs were displaced consistently with CMR data and a physiological transvalvular pressure drop, up to 120 mmHg, was applied on the ventricular side of the leaflets throughout a 1.0 s timeframe.

RESULTS

Simulation-H

In the healthy valve, complete leaflets coaptation occurred at a very low value of transvalvular pressure

drop: when a 15 mmHg value was reached, the valve orifice was already occluded. After reaching 60 mmHg of transvalvular pressure drop, the valve underwent only minor further deformations, mostly associated with the motion of the annulus and PMs, and achieved a coaptation length, measured on the mid-section passing through the saddle horn and midpoint of the posterior annulus, equal to 6.1 mm.

Leaflets deformations at PS reflected the anisotropy of material properties (Fig. 4). In the circumferential direction, strains were higher in the mid-region of the anterior leaflet ($13 \div 16\%$), decreased towards the trigones (5%) and became compressive at the commissures (-12%). The posterior leaflet underwent tensile strains in the belly region of the central cusp (6%), while the annular region experienced heterogeneous compressive strains ($-6 \div -14\%$) due to annular contraction. In the radial direction strains were about $25 \div 30\%$ in the anterior leaflet belly, increasing up to 45% near the trigones, while they ranged from 35 to 45% in the posterior leaflet cusps.

Leaflets maximum principal stresses at PS (Fig. 5, Sim-H) showed an asymmetric distribution. The region close to the fibrous trigones was the most stressed one, with peak values equal to 430 kPa. The anterior annular region also showed high tensile values (about 300 kPa), while stresses decreased towards the free margin. The posterior leaflet showed considerably lower stresses than the anterior one, with a maximum of about 120 kPa.

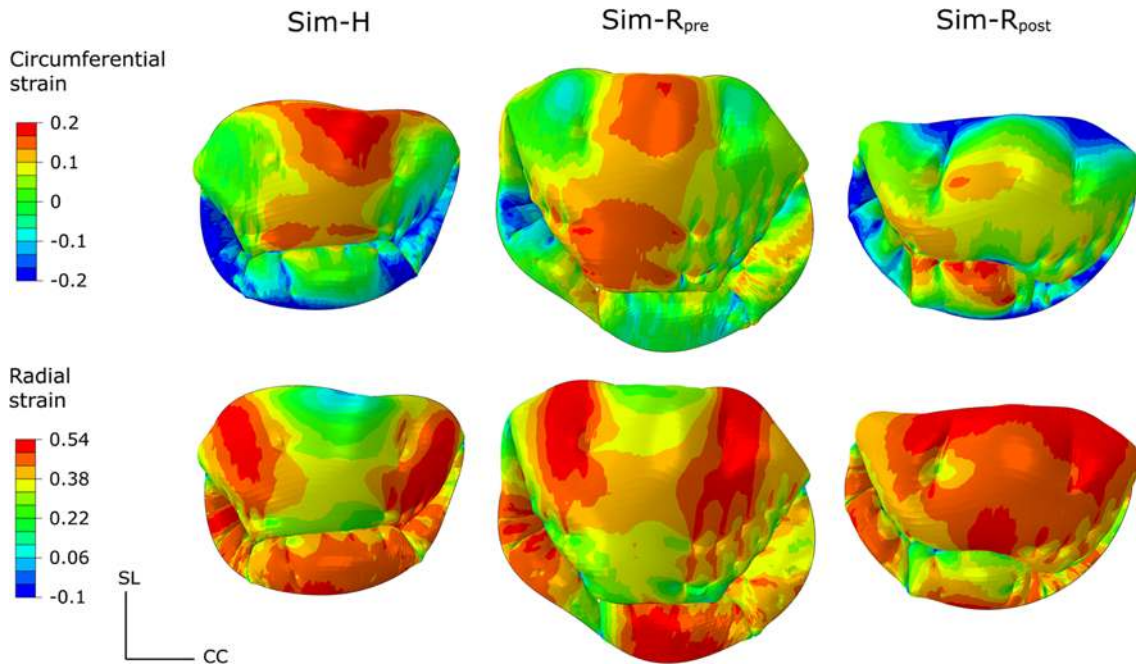


FIGURE 4. Distribution of circumferential and radial strains on the leaflets at the systolic peak (atrial view, CC = commissure-commissural direction, SL = septo-lateral direction) for the simulated healthy valve (Sim-H), regurgitant valve (Sim- R_{pre}) and repaired valve (Sim- R_{post}).

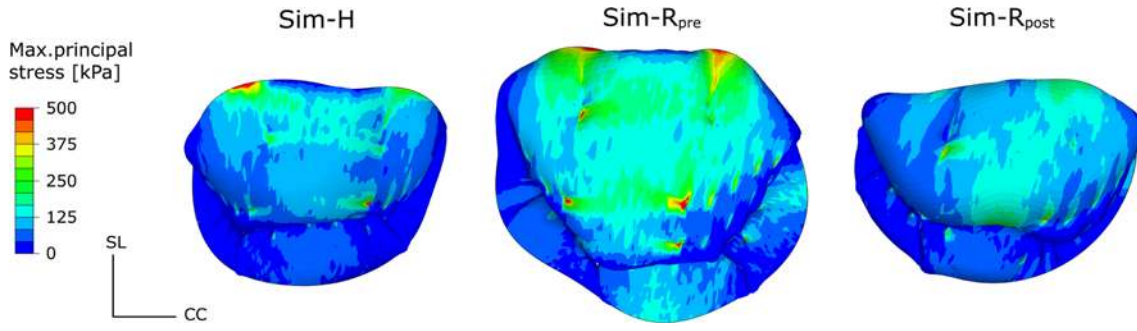


FIGURE 5. Maximum principal stress distribution on the leaflets at the systolic peak (atrial view, CC = commissure-commissural direction, SL = septo-lateral direction) for the simulated healthy valve (Sim-H), regurgitant valve (Sim-R_{pre}) and repaired valve (Sim-R_{post}).

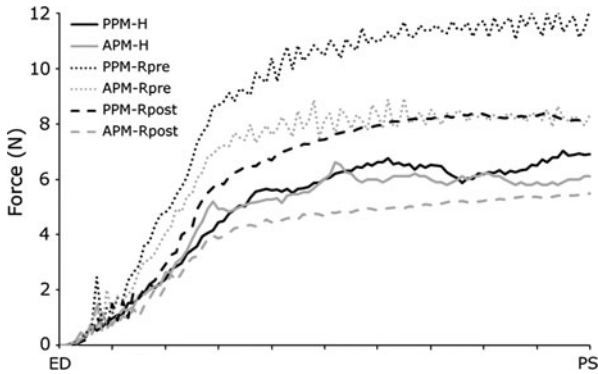


FIGURE 6. Time course of the force acting on the antero-lateral PM (APM, grey) and on the posteromedial PM (PPM, black) in simulation-H (continuous line), simulation-R_{pre} (dotted line) and simulation-R_{post} (dashed line).

As regards tensions in the subvalvular apparatus, PM reaction force evolved during closure following the transvalvular pressure (Fig. 6). Peak force values were 6.11 N and 6.92 N on the anterolateral and posteromedial PM, respectively. These forces were unevenly transmitted to the chordae tendineae throughout the simulated time course (Table 1), and the average load on a single chorda was highest in the strut chordae (up to 0.9 N at PS).

Regional forces acting on the annulus were evaluated at PS as a function of the position along the annulus (Fig. 7). Reaction forces were highest near the fibrous trigones, with peak values of about 45 mN, and decreased near the saddle horn. On the posterior annulus, reaction forces were lower, with a maximum value of 22 mN located at the posterior annulus mid-point, while forces at the commissures and paracommissures were almost zero.

Simulations R_{pre} and R_{post}

In the regurgitant valve, coaptation was incomplete and two regurgitant areas were identified near the paracommissures, consistently with CMR images and leaflets profile as reconstructed through our software at PS (Fig. 8).

After annuloplasty, full coaptation was restored for a transvalvular pressure drop equal to 16 mmHg. After the insertion of the annuloplasty ring, the coaptation length, that was almost zero in simulation-R_{pre}, increased to 9.3 mm, 50% higher than in the healthy scenario (Fig. 9).

Maximum principal stresses on the leaflets before surgery (Fig. 5, Sim-R_{pre}) showed peak values of almost 500 kPa next to the fibrous trigones and near the

TABLE 1. Chordae tendineae forces (mean value \pm standard deviation) obtained at PS for different chordal types in the three simulated configurations.

	No.	sim-H	sim-R _{pre}	sim-R _{post}
Marginal				
Anterior	10	0.142 \pm 0.072	0.246 \pm 0.192	0.193 \pm 0.091
Posterior	10	0.182 \pm 0.050	0.266 \pm 0.119	0.304 \pm 0.176
Basal				
Anterior	20	0.225 \pm 0.119	0.412 \pm 0.303	0.216 \pm 0.148
Posterior	20	0.088 \pm 0.047	0.191 \pm 0.092	0.106 \pm 0.075
Commissural	2	0.153	0.279	0.140
Paracommissural	2	0.239	0.372	0.245
Strut	2	0.898	1.197	0.824

Values are expressed in N.

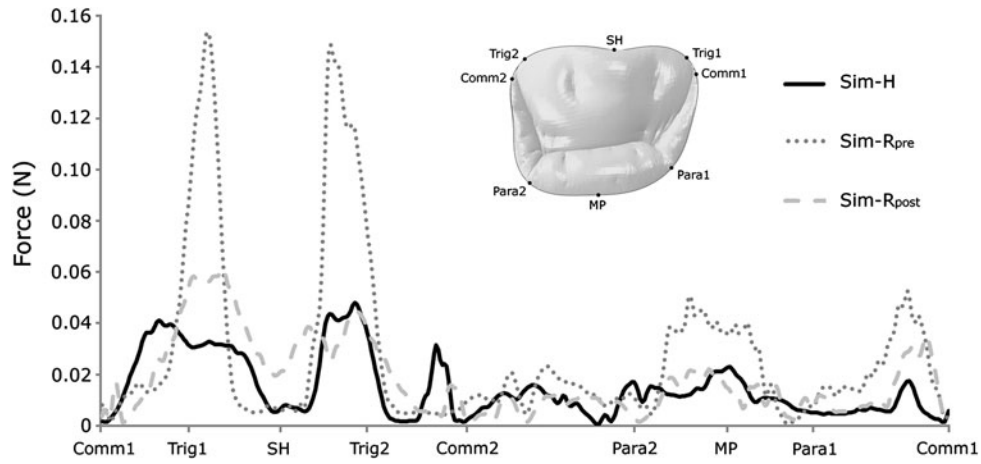


FIGURE 7. Regional annular forces as a function of the position along the annulus for simulation-H (black continuous line), simulation- R_{pre} (grey dotted line) and simulation- R_{post} (grey dashed line). Comm = commissure, Trig = trigone, SH = saddle horn, MP = posterior annulus midpoint.

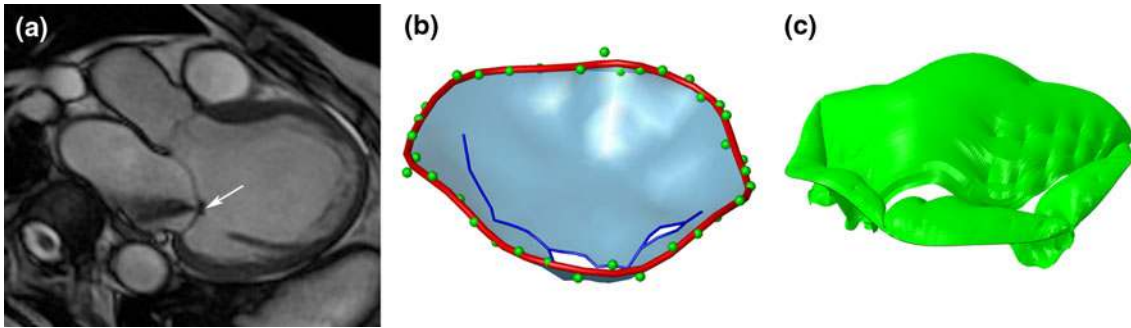


FIGURE 8. (a) MV regurgitant jet at peak systole as visible in the CMR cut-plane passing through the saddle horn and the midpoint of the posterior annulus; (b) corresponding leaflet surface reconstructed through our software. Two regurgitant areas are visible; (c) Approximately the same areas are visible in the same three-dimensional view of MV leaflets obtained at systolic peak in simulation- R_{pre} .

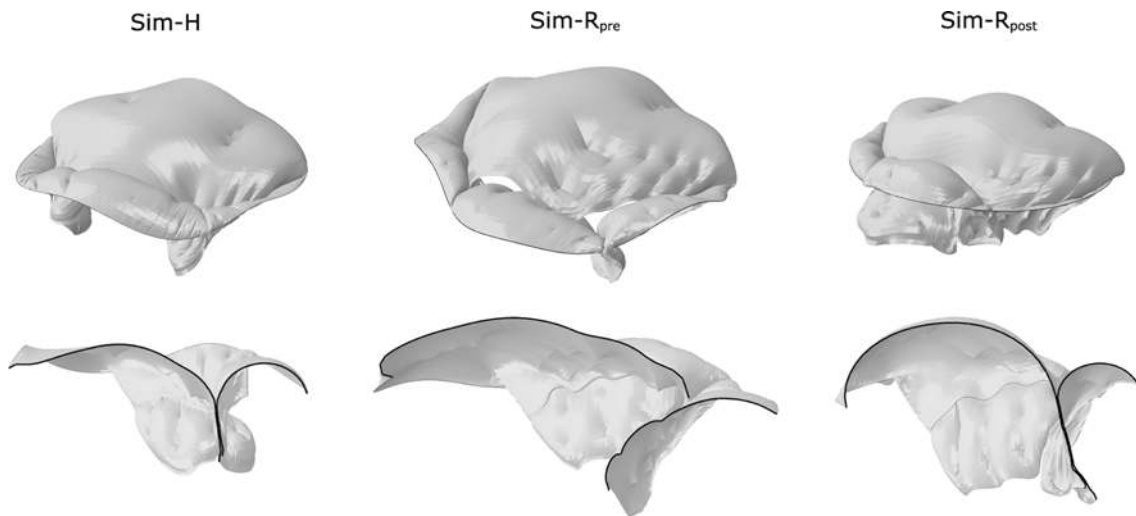


FIGURE 9. Three-dimensional view of leaflets in closed configuration (top) and cross-section passing through the saddle horn and the posterior annulus midpoint (bottom) for the three simulations.

insertion zones of the strut chordae. Also, both anterior and posterior leaflets were overall more stressed than in the healthy case (300 and 150 kPa, respectively). Stress values after MV repair (Fig. 5, Sim- R_{post}) were globally lower, and much closer to the ones in simulation-H. On the anterior leaflet, stresses were highest near the trigones and in the belly (230 kPa), while maximum stress on the posterior leaflet was equal to 80 kPa.

Forces acting on the PMs in the regurgitant valve were much higher than in the healthy one (Fig. 6), with systolic peak values of 12.1 N on the postero-medial PM and of 8.3 N on the antero-lateral PM (+75% and +36% with respect to the corresponding healthy values). These values were remarkably decreased by the simulated repair procedure, which lowered reaction forces on both PMs by about 33%. This effect was reflected on the chordal forces that decreased in all the different orders to the level of the healthy scenario, with the only exception of the posterior marginal chordae (Table 1).

Annular forces distribution (Fig. 7) in simulation- R_{pre} showed marked peaks next to the trigones (150 mN) and high values near the posterior annulus midpoint and the posteromedial commissure. In simulation- R_{post} the use of a rigid annuloplasty ring relieved the annulus almost halving these peaks. In particular, the forces concentrated at the trigones in simulation- R_{pre} were distributed across the intertrigonal region, causing a sensible increase in the force acting at the saddle horn in simulation- R_{post} .

DISCUSSION

We presented a method to implement patient-specific FEMs of the MV from CMR, and tested it on one healthy subject and on one ischemic patient with MR. In order to extensively test the robustness of our approach and to infer sound conclusions about MV biomechanics in the different simulated scenarios, our analysis should be extended to a much wider set of subjects, and data of statistical significance should be gathered. Still, our preliminary simulations suggest some conclusions.

Simulation-H: Reliability of the Modelling Procedure

Several experimental data about healthy MV function are available from the scientific literature. The results from simulation-H were used to validate our modelling strategy: good agreement was found relevant to several aspects of MV biomechanics, thus supporting the validity of our approach. Complete

closure of the valve was achieved with a 15 mmHg transvalvular pressure, consistent with the *in vivo* value of about 20 mmHg reported in Timek *et al.*²²; in agreement with clinical observations, the coaptation region corresponded to the leaflets rough zone. The overall distribution of leaflets maximum principal stresses at PS agreed with the one reported in Votta *et al.*²⁴: as in that study, peak values were observed next to the trigones, acting as anchoring points, even if the more detailed regional leaflets thickness pattern we introduced into the model toned down this value (from 550 to 430 kPa). Leaflets strains in the central region of the anterior leaflet matched *in vitro* values provided in Sacks *et al.*,²⁰ equal to 1.11 ± 0.04 in circumferential direction and 1.32 ± 0.08 in radial direction. Tensions in the subvalvular apparatus were consistent with *in vitro* values reported by Jimenez and colleagues,⁷ who measured a peak systolic tension equal to 0.95 ± 0.35 N on strut chordae, 0.11 ± 0.20 N on commissural chordae and 0.23 ± 0.19 N on marginal chordae.

The only notable discrepancy with respect to real MV function was in the shape assumed by the anterior leaflet in the closed valve configuration. In fact, in our simulation the anterior leaflet became concave towards the ventricle and its belly markedly bulged into the atrium, while *in vivo* it is characterized by a compound shape and by the absence of bulging. Such limitation was probably due to the assumption of passive mechanical properties for the leaflets: the active contraction of smooth muscle and interstitial cells, which increases leaflets stiffness even by orders of magnitude and drives systolic anterior leaflet compound shape *in vivo*,^{9–11} was neglected. Accounting for anterior leaflet active response will be a mandatory improvement of our work, possibly following the approach proposed in Skallerud *et al.*²¹

As regards the use of CMR as source of data, it allowed some improvements to be obtained with respect to our previous approach based on TT-RT3DE: high spatial and temporal resolutions allowed to accurately describe not only the shape of the annulus, but also the PM position in each time-frame, thus overcoming the limitations in the definition of time-varying PM displacements when using TT-RT3DE.²⁴ CMR may also allow for more flexibility and precision in the modelling procedure, since image quality is not affected by the quality of the acoustic window and, thanks to steady-state free precession (SSFP) sequences, has a better temporal resolution. On the other hand, CMR is not as routinely used as TT-RT3DE in the analysis of MV function and in any case the rotational acquisition we adopted in this study was set *ad hoc* and is not commonly used in the study of MV apparatus. Given the long-term goal of our

work, i.e. the development of a decision-support tool for clinical use, this is a limitation worth considering.

Simulations R_{pre} and R_{post} : Application to Annuloplasty Procedures

Results from simulation- R_{pre} suggest that the proposed modeling strategy is sensitive enough to reproduce extent and location of MV regurgitation at PS, as well as alterations in MV biomechanics, associated to pathological MV morphology. These consisted in a marked increase in force values in the sub-valvular apparatus and in stresses observed on the leaflets, particularly in the fibrous trigone region. These outcomes are consistent with the lack of coaptation characterizing the simulated pathological condition.

However, it is worth noting that, due to the impossibility to measure leaflets thickness from clinical images, we assigned a standard thickness distribution proposed in the literature¹⁵ for healthy MVs, also when simulating the regurgitant MV. This assumption may be acceptable for the specific pathological scenario considered in the present study, but could not be adopted for other scenarios characterized by important alterations of leaflet thickness (e.g. mixomatous disease). Since the long-term goal of our work is the development of a flexible modeling strategy, this simplifying assumption will need to be removed or modified in the future. To this purpose, disease-related criteria to modulate leaflets thickness will have to be identified from *ex vivo* measurements and literature data.

Results from sim- R_{post} suggested that, besides restoring MV continence, undersized rigid annuloplasty can have two other positive effects: (1) by restoring normal systolic peak leaflets stresses in the fibrous trigones region, where abnormal values were observed in sim- R_{pre} . This outcome is consistent with Kunzelman *et al.*,¹⁴ where this beneficial effect was less evident but annuloplasty was modelled without considering undersizing; (2) tensions in the sub-valvular apparatus are reduced, consistently with the fact that undersized annuloplasty decreases the surface of the MV orifice. In this way, the area on which the ventricular pressure acts pushing the leaflets toward the atrium is reduced and, consequently, the load counterbalanced by PM traction is decreased. Moreover, thanks to restored coaptation, MV leaflets partially sustain each other. Of course, the drawback of the procedure is in the lack of annular dynamics in the post-operative scenario.

Unfortunately, these results, although reasonable according to a rule of thumb, cannot be compared to an *in vivo* counterpart, since follow-up data of the patient whose regurgitant valve was modelled were not available.

Again, besides the possible clinical implications of our findings, some considerations can be done on the potential of the method. Here we have shown the simulation of rigid annuloplasty by imposing the prosthetic ring shape to the native annulus and then maintaining it throughout early systole, which was the simulated part of the cardiac cycle. This approach could not be adopted if flexible annuloplasty had to be simulated, since in that case the ring shape could change dynamically due to the forces imposed by myocardial contraction. A possible alternative approach that we are planning to use to include that application into our modelling strategy would imply to (i) explicitly include the prosthetic ring into the model and (ii) impose as boundary conditions on annular nodes the time-dependent nodal forces calculated at the annulus for the pathological configuration.

Another aspect worth discussing is the systolic peak configuration of MV leaflets in sim- R_{post} . As in simulation-H, this is characterized by a pronounced bulging of the anterior leaflet into the atrium, that is likely caused by having neglected leaflets active stiffening. Thus, in its current version our model may be used to predict MV post-operative continence as it would be assessed by surgeons in the operative room before decannulation (i.e. by pressurizing the left ventricle with saline solution and observing consequent leaflets closure). This is already a useful information, however it would be more interesting to predict the real one, i.e. beating heart, post-operative configuration and curvature of MV leaflets, which are strictly related to MV function and resistance to pressure loads, and thus, presumably, to the long-term durability of the surgical correction. From this standpoint, accounting for the contractile properties of anterior leaflet tissue is confirmed to be a mandatory refinement of our modelling strategy.

One last consideration regards the time needed for the entire modeling process, from image processing to FEM results post-processing. On a standard personal computer and for a non-expert user, our software allows CMR images to be processed in 1–1.5 h and FEM set-up in 5–10 min. The numerical solution of the simulations required from 13 h (simulation-H) to 23 h (simulation- R_{post}) on an 8-CPU parallel computing system. Thus, the whole process needs to become faster in order to be compatible with the clinical practice. At this purpose the CMR image processing software shall become as automated as possible, so to reduce the need for user's interaction. Simulations' computational costs shall be reduced by increasing the number of CPUs, and by optimizing the discretization of the MV geometry, since the performance of explicit solvers as the one herein adopted is very sensitive to the size of the finite elements.

CONCLUSIONS

In this study we presented the results of our first steps towards the long-term goal of developing a decision-support tool for MV surgery, based on CMR image processing and patient-specific finite element modeling. Our results suggest the feasibility of this approach and highlight the developments needed to satisfy the requirements for its clinical application, i.e. flexibility, usability and time-efficiency.

ACKNOWLEDGMENT

The research leading to these results has received funding from the European Community's Seventh Framework Programme (FP7/2007-2013) under Grant Agreement No. 224635.

REFERENCES

- ¹Arnoldi, A., A. Invernizzi, R. Ponzini, E. Votta, E. G. Caiani, and A. Redaelli. Mitral valve models reconstructor: a Python based GUI software in a HPC environment for patient-specific FEM structural analysis. *Innovations and Advances in Computer Sciences and Engineering*, Netherlands: Springer, 2010, pp. 215–219.
- ²Avanzini, A. A computational procedure for prediction of structural effects of edge-to-edge repair on mitral valve. *J. Biomech. Eng.* 130(3):031015, 2008.
- ³Bothe, W., J. P. Kvitting, J. C. Swanson, S. Hartnett, N. B. Ingels, Jr., and D. C. Miller. Effects of different annuloplasty rings on anterior mitral leaflet dimensions. *J. Thorac. Cardiovasc. Surg.* 139(5):1114–1122, 2010.
- ⁴Bouma, W., I. C. van der Horst, I. J. Wijdh-den Hamer, M. E. Erasmus, F. Zijlstra, M. A. Mariani, and T. Ebels. Chronic ischaemic mitral regurgitation. Current treatment results and new mechanism-based surgical approaches. *Eur. J. Cardiothorac. Surg.* 37(1):170–185, 2010.
- ⁵Gammie, J. S., S. Sheng, B. P. Griffith, E. D. Peterson, J. S. Rankin, S. M. O'Brien, and J. M. Brown. Trends in mitral valve surgery in the United States: results from the Society of Thoracic Surgeons Adult Cardiac Surgery Database. *Ann. Thorac. Surg.* 87(5):1431–1437, 2009; discussion 1437–1439.
- ⁶Hung, J., L. Papakostas, S. A. Tahta, B. G. Hardy, B. A. Bollen, C. M. Duran, and R. A. Levine. Mechanism of recurrent ischemic mitral regurgitation after annuloplasty: continued LV remodeling as a moving target. *Circulation* 110(11 Suppl 1):II85–II90, 2004.
- ⁷Jimenez, J. H., D. D. Soerensen, Z. He, S. He, and A. P. Yoganathan. Effects of a saddle shaped annulus on mitral valve function and chordal force distribution: an in vitro study. *Ann. Biomed. Eng.* 31(10):1171–1181, 2003.
- ⁸Kaji, S., M. Nasu, A. Yamamuro, K. Tanabe, K. Nagai, T. Tani, K. Tamita, K. Shiratori, M. Kinoshita, M. Senda, Y. Okada, and S. Morioka. Annular geometry in patients with chronic ischemic mitral regurgitation: three-dimensional magnetic resonance imaging study. *Circulation* 112(9 Suppl):I409–I414, 2005.
- ⁹Krishnamurthy, G., D. B. Ennis, A. Itoh, W. Bothe, J. C. Swanson, M. Karlsson, E. Kuhl, D. C. Miller, and N. B. Ingels, Jr. Material properties of the ovine mitral valve anterior leaflet in vivo from inverse finite element analysis. *Am. J. Physiol. Heart Circ. Physiol.* 295(3):H1141–H1149, 2008.
- ¹⁰Krishnamurthy, G., A. Itoh, J. C. Swanson, W. Bothe, M. Karlsson, E. Kuhl, D. Craig Miller, and N. B. Ingels, Jr. Regional stiffening of the mitral valve anterior leaflet in the beating ovine heart. *J. Biomech.* 42(16):2697–2701, 2009.
- ¹¹Krishnamurthy, G., A. Itoh, J. C. Swanson, D. C. Miller, and N. B. Ingels, Jr. Transient stiffening of mitral valve leaflets in the beating heart. *Am. J. Physiol. Heart Circ. Physiol.* 298(6):H2221–H2225, 2010.
- ¹²Kunzelman, K. S., and R. P. Cochran. Mechanical properties of basal and marginal mitral valve chordae tendineae. *ASAIO Trans.* 36(3):M405–M408, 1990.
- ¹³Kunzelman, K. S., D. W. Quick, and R. P. Cochran. Altered collagen concentration in mitral valve leaflets: biochemical and finite element analysis. *Ann. Thorac. Surg.* 66(6 Suppl):S198–S205, 1998.
- ¹⁴Kunzelman, K. S., M. S. Reimink, and R. P. Cochran. Flexible versus rigid ring annuloplasty for mitral valve annular dilatation: a finite element model. *J. Heart Valve Dis.* 7(1):108–116, 1998.
- ¹⁵Kunzelman, K. S., D. R. Einstein, and R. P. Cochran. Fluid-structure interaction models of the mitral valve: function in normal and pathological states. *Philos. Trans. R. Soc. Lond. B. Biol. Sci.* 362(1484):1393–1406, 2007.
- ¹⁶Lam, J. H., N. Ranganathan, E. D. Wigle, and M. D. Silver. Morphology of the human mitral valve. I. Chordae tendineae: a new classification. *Circulation* 41(3):449–458, 1970.
- ¹⁷May-Newman, K., and F. C. Yin. A constitutive law for mitral valve tissue. *J. Biomech. Eng.* 120(1):38–47, 1998.
- ¹⁸McGee, E. C., A. M. Gillinov, E. H. Blackstone, J. Rajeswaran, G. Cohen, F. Najam, T. Shiota, J. F. Sabik, B. W. Lytle, P. M. McCarthy, and D. M. Cosgrove. Recurrent mitral regurgitation after annuloplasty for functional ischemic mitral regurgitation. *J. Thorac. Cardiovasc. Surg.* 128(6):916–924, 2004.
- ¹⁹Prot, V., B. Skallerud, G. Sommer, and G. A. Holzapfel. On modelling and analysis of healthy and pathological human mitral valves: two case studies. *J. Mech. Behav. Biomed. Mater.* 3(2):167–177, 2010.
- ²⁰Sacks, M. S., Z. He, L. Baijens, S. Wanant, P. Shah, H. Sugimoto, and A. P. Yoganathan. Surface strains in the anterior leaflet of the functioning mitral valve. *Ann. Biomed. Eng.* 30(10):1281–1290, 2002.
- ²¹Skallerud, B., V. Prot, and I. S. Nordrum. Modeling active muscle contraction in mitral valve leaflets during systole: a first approach. *Biomech. Model. Mechanobiol.* 2010. doi: 10.1007/s10237-010-0215-9.
- ²²Timek, T., J. R. Glasson, P. Dagum, G. R. Green, J. F. Nistal, M. Komeda, G. T. Daughters, A. F. Bolger, L. E. Foppiano, N. B. Ingels, Jr., and D. C. Miller. Ring annuloplasty prevents delayed leaflet coaptation and mitral regurgitation during acute left ventricular ischemia. *J. Thorac. Cardiovasc. Surg.* 119(4 Pt 1):774–783, 2000.
- ²³Votta, E., F. Maisano, S. F. Bolling, O. Alfieri, F. M. Montevicchi, and A. Redaelli. The Geoform disease-specific annuloplasty system: a finite element study. *Ann. Thorac. Surg.* 84(1):92–101, 2007.

²⁴Votta, E., E. Caiani, F. Veronesi, M. Soncini, F. M. Montecvecchi, and A. Redaelli. Mitral valve finite-element modelling from ultrasound data: a pilot study for a new approach to understand mitral function and clinical scenarios. *Philos. Trans. R. Soc. A Math. Phys. Eng. Sci.* 366(1879):3411–3434, 2008.

²⁵Yu, H. Y., M. Y. Su, T. Y. Liao, H. H. Peng, F. Y. Lin, and W. Y. Tseng. Functional mitral regurgitation in chronic ischemic coronary artery disease: analysis of geometric alterations of mitral apparatus with magnetic resonance imaging. *J. Thorac. Cardiovasc. Surg.* 128(4): 543–551, 2004.